Mapping the Interactions of the p53 Transactivation Domain with the KIX Domain of CBP[†]

Chul Won Lee,[‡] Munehito Arai,[‡,§] Maria A. Martinez-Yamout,[‡] H. Jane Dyson,[‡] and Peter E. Wright*[,‡]

Department of Molecular Biology and The Skaggs Institute for Chemical Biology, The Scripps Research Institute, 10550 North Torrey Pines Road, La Jolla, California 92037, and Institute for Biological Resources and Functions, National Institute of Advanced Industrial Science and Technology (AIST), 1-1-1 Higashi, Tsukuba, Ibaraki 305-8566, Japan

Received November 4, 2008; Revised Manuscript Received January 9, 2009

ABSTRACT: Molecular interactions between the tumor suppressor p53 and the transcriptional coactivators CBP/p300 are critical for the regulation of p53 transactivation and stability. The transactivation domain (TAD) of p53 binds directly to several CBP/p300 domains (TAZ1, TAZ2, NCBD, and KIX). Here we map the interaction between the p53 TAD and the CBP KIX domain using isothermal titration calorimetry and NMR spectroscopy. KIX is a structural domain in CBP/p300 that can simultaneously bind two polypeptide ligands, such as the activation domain of MLL and the kinase-inducible activation domain (pKID) of CREB, using distinct interaction surfaces. The p53 TAD consists of two subdomains (AD1 and AD2); peptides corresponding to the isolated AD1 and AD2 subdomains interact with KIX with relatively low affinity, but a longer peptide containing both subdomains binds KIX tightly. In the context of the full-length p53 TAD, AD1 and AD2 bind synergistically to KIX. Mapping of the chemical shift perturbations onto the structure of KIX shows that isolated AD1 and AD2 peptides bind to both the MLL and pKID sites. Spin-labeling experiments show that the complex of the full-length p53 TAD with KIX is disordered, with the AD1 and AD2 subdomains each interacting with both the MLL and pKID binding surfaces. Phosphorylation of the p53 TAD at Thr18 or Ser20 increases the KIX binding affinity. The affinity is further enhanced by simultaneous phosphorylation of Thr18 and Ser20, and the specificity of the interaction is increased. The p53 TAD simultaneously occupies the two distinct sites that have been identified on the CBP KIX domain and efficiently competes for these sites with other known KIX-binding transcription factors.

Eukaryotic transcriptional regulation is accomplished through a complex network of interactions between gene-specific DNA-bound activators and coactivators. CREB binding protein (CBP)[1] and its close relative p300 are general transcriptional coactivators that function as scaffolds for the recruitment and assembly of the transcriptional machinery and also modify chromatin and transcription factors through their intrinsic acetyltransferase activity (*1*). CBP and p300 contain a number of modular protein binding domains that mediate recruitment by a diverse array of transcription factors.

The KIX domain was first characterized as the region of CBP responsible for binding the phosphorylated kinase-inducible activation domain (pKID) of CREB (*2*). Many other eukaryotic and viral transcription factors, including MLL, c-Jun, c-Myb, HTLV-1 Tax, and HIV-1 Tat, have since been shown to recruit CBP/p300 through interactions with the KIX domain (*1, 3*−*8*). The NMR structure of the KIX·pKID complex (*9*) revealed that pKID folds upon binding to KIX, forming two orthogonal α-helices. The αB helix of pKID binds to a hydrophobic groove formed by the first and third helices of KIX while the αA helix of pKID interacts with a different face of the third helix. The c-Myb activation domain binds to the same hydrophobic groove as the αB helix of pKID (*10*). However, the activation domains of MLL, Tax, Tat, and c-Jun bind to a different surface of KIX, on the opposite face of the protein from the pKID/c-Myb binding site (*8, 11*−*13*). The existence of two distinct binding surfaces means that KIX is capable of binding two transcriptional activation domains simultaneously to form a ternary complex. Simultaneous, cooperative binding of MLL and pKID or MLL and c-Myb to KIX (*12*) provides a potential mechanism for synergism between different transcriptional pathways. It has recently been suggested that the human T-cell leukemia virus (HTLV-1) oncoprotein Tax participates in oncogenesis by competing with MLL for KIX

[†] This work was supported by Grant CA96865 from the National Institutes of Health and by The Skaggs Institute for Chemical Biology. C.W.L. was supported by the Korea Research Foundation grant funded by the Korean Government (MOEHRD, Basic Research Promotion Fund) (KRF-2004-214-C00207) and by a Skaggs training grant.

* Corresponding author. E-mail: wright@scripps.edu. Telephone: (858) 784-9721. Fax: (858) 784-9822.

[‡] The Scripps Research Institute.

[§] National Institute of Advanced Industrial Science and Technology.

[1] Abbreviations: CREB, cyclic-AMP response element binding protein; CBP, CREB-binding protein; DSS, sodium 2,2-dimethyl-2-silapentane-5-sulfonate; HSQC, heteronuclear single-quantum coherence; ITC, isothermal titration calorimetry; MDM2, mouse double minute protein 2; MLL, mixed lineage leukemia protein; MTSL, (1-oxy-2,2,5,5-tetramethyl-Δ^3-pyrrolin-3-yl)methyl methanethiosulfonate; NCBD, nuclear receptor coactivator binding domain; NMR, nuclear magnetic resonance; pKID, phosphorylated kinase-inducible domain; TAZ, transcriptional adapter zinc finger.

10.1021/bi802055v CCC: $40.75
Published on Web 02/16/2009

binding, in order to recruit CBP/p300 to the viral HTLV-1 promoter (*14*).

The tumor suppressor p53 plays crucial roles in cell cycle arrest and apoptosis in response to stress stimuli such as oncogene activation or DNA damage (*15, 16*). The stabilization, transactivation, and DNA binding activity of p53 are regulated through physical and functional interactions with CBP/p300 (*17, 18*). The N-terminal region of p53 contains a transcriptional activation domain (TAD, residues 1−61) and a proline-rich domain (residues 62−91), both of which are intrinsically disordered (*19*−*21*). Two subdomains within the TAD, termed AD1 (residues 1−40) and AD2 (residues 41−61), mediate protein−protein interactions that regulate the stability of p53 and activate transcription of p53 responsive genes (*22*−*25*). The p53 TAD mediates interactions with multiple domains of CBP/p300 and is essential for transactivation of p53-responsive genes (*26*−*34*).

Here we focus on the interactions between the p53 TAD and the KIX domain of CBP/p300, which have been shown to be important for p53 transactivation (*31*). The HTLV-1 oncoprotein Tax also binds to the KIX domain (*35, 36*) and inhibits p53-mediated transactivation (*37*) or alleviates p53-induced repression of target genes (*38*). To obtain insights into the nature of the complex formed between the p53 TAD and KIX, we have used NMR methods to map the interactions of the full-length TAD and the isolated AD1 and AD2 subdomains to the KIX domain of CBP. While binding of isolated AD1 and AD2 to KIX was not detectable using ITC, interactions were observed by NMR, allowing calculation of dissociation constants for binding of the individual subdomains. A much tighter interaction was observed for the full-length p53 TAD than the isolated AD1 and AD2 subdomains, although the complex is structurally disordered. Phosphorylation of the p53 TAD at Thr18 and/or Ser20 significantly enhances the affinity and specificity of the interaction with KIX.

EXPERIMENTAL PROCEDURES

Protein Expression and Sample Preparation. Constructs corresponding to residues 38−61, 13−61, and 1−61 of human p53 protein were generated by PCR-based mutagenesis. All p53 TAD constructs were expressed as N-terminal fusions with His_6-GB1 (residues 1−56 of the B1 domain of protein G) in *Escherichia coli* BL21(DE3)[DNAY]. Pellets containing p53 TAD peptides were suspended in 40 mL of buffer (6 M urea, 25 mM Tris-HCl, pH 8.0, 150 mM NaCl) per liter of culture. The soluble fraction was isolated by centrifugation at 20000*g* for 30 min. The supernatant was purified by chromatography on Ni-NTA resin, and the His_6-GB1 tag was removed by thrombin digestion in the column. The cleaved p53 constructs were further purified by reversed-phase HPLC.

The activation domains of MLL (residues 2842−2869), pKID (residues 114−147), and c-Myb (residues 284−315) were prepared from GB1 fusion proteins as described previously (*39*). The KIX domain (residues 586−672) of mouse CBP was expressed and purified as previously described (*9*). Samples were prepared with ^{15}N labeling and ^{15}N,^{13}C double labeling for NMR experiments. A peptide containing residues 14−28 of human p53, designated p53(14−28), was synthesized on a Perseptive Biosystems synthesizer using standard solid-phase Fmoc methods. The phosphorylated peptides p53(13−57)pT18, p53(13−57)pS20, and p53(13−57)pT18pS20, were synthesized using Fmoc-Thr(PO(OBzl)-OH)-OH and Fmoc-Ser(PO(OBzl)-OH)-OH for incorporation of phosphothreonine and phosphoserine, respectively. The peptides were purified with reversed-phase HPLC on a C18 silica column, and purity and mass were confirmed by analytical reversed-phase HPLC and MALDI-TOF.

Preparation of Spin-Labeled Samples. Single N-terminal (P13C) and C-terminal (D61C) cysteine mutants were generated from the His_6-GB1-p53(13−61) plasmid using the QuikChange kit (Stratagene). An additional residue (Gly) was incorporated at the N-terminus to facilitate thrombin cleavage from the His_6-GB1 tag. The purification protocol was slightly modified for the spin-labeled protein. Bacterial pellets were suspended in 40 mL of 6 M urea, 25 mM Tris-HCl, pH 8.0, 150 mM NaCl, and 10 mM β-mercaptoethanol. The lysis supernatant was loaded onto Ni-NTA resin, and the resin was washed with lysis buffer without β-mercaptoethanol. A 5-fold molar excess of MTSL (Toronto Research Chemicals) was added to the Ni-NTA resin and incubated at room temperature for ~12 h. The His_6-GB1 tag was removed by cleavage with thrombin in 25 mM Tris-HCl buffer, pH 8.0, containing 150 mM NaCl. The spin-labeled protein was eluted from the column and purified by reversed-phase HPLC. Attachment of the spin label was confirmed by MALDI-TOF (Supporting Information Figure S1).

The phosphorylated cysteine mutant peptides p53(13−57)pT18pS20(P13C) and p53(13−57)pT18pS20(D57C) were synthesized using standard solid-phase Fmoc methods and purified by reversed-phase HPLC. The purified peptides were lyophilized and resuspended in 20 mM Tris-HCl, pH 8.0, 50 mM NaCl, and 5 mM DTT to a concentration of approximately 4 mg/mL. DTT was removed by buffer exchange on a NAP10 column (GE Healthcare), and the protein was immediately labeled with MTSL. A 10-fold molar excess of MTSL was added, and the reaction was allowed to proceed for ~12 h at room temperature. The spin-labeled p53 peptides were purified by reversed-phase HPLC. Attachment of the spin label was confirmed by MALDI-TOF (Supporting Information Figure S2).

Isothermal Titration Calorimetry (ITC). ITC experiments were performed at 35 °C using a MicroCal Omega VP-ITC instrument (MicroCal, Amherst, MA). Samples were prepared in 50 mM Tris-HCl, pH 7.0, and 50 mM NaCl buffer. Protein concentration was determined by absorbance at 280 nm. The concentration of KIX in the ITC cell was 50 μM; the concentrations of the p53 peptides in the syringe were 10-fold greater than that of KIX. Typically, one injection of 5 μL was followed by 29 injections of 10 μL until a molar ratio of 2.5 was obtained. The dilution heats are typically small and were subtracted from the calorimetric data. Integration of the thermogram and subtraction of the blanks yielded a binding isotherm that was fitted to a one-site binding model using the Microcal Origin software. The stoichiometry for the ITC runs ranged from 0.8 to 1.2, with most close to 1.0. All experiments were performed in duplicate.

NMR Spectroscopy. NMR spectra were recorded at 27 °C on Bruker Avance500 and DRX600 spectrometers fitted with cryoprobes and were referenced to external DSS. Protein samples were prepared in NMR buffer (20 mM Tris-HCl,

pH 6.5, 50 mM NaCl) at concentrations of 0.2−0.5 mM for labeled protein samples and 0.02−1 mM for unlabeled proteins. NMR data processing and analysis were performed using NMRPipe (*40*) and NMRView (*41*). Backbone resonances of KIX and p53(13−61) were assigned using standard triple-resonance experiments: HNCA (*42*), HNCACB (*43*), and CBCA(CO)NH (*42*).

Spin-labeled NMR samples were prepared in NMR buffer at a molar ratio of 1:1 for ^{15}N- labeled KIX and spin-labeled p53 peptides. For measurements of paramagnetic relaxation enhancement, ^{1}H−^{15}N HSQC spectra were recorded in the presence and absence of ascorbic acid. Reduction of the spin label to its diamagnetic state was achieved by addition of a 5-fold molar excess of ascorbic acid and incubation overnight. The intensity ratios of ^{1}H−^{15}N HSQC peaks were calculated as I_{para}/I_{dia}, where I_{para} is the resonance intensity of the spin-labeled sample, I_{dia} is the resonance intensity of the spin-labeled sample following reduction by ascorbic acid. In control experiments, free MTSL spin label added to KIX caused no detectable broadening of resonances in the HSQC spectrum (Supporting Information Figure S3).

Dissociation Constants from Chemical Shift Titrations. The dissociation constant, K_d, was obtained from changes in the weighted average chemical shift differences $\Delta\delta(N,H)_{av} = [(\Delta\delta_{HN})^2 + (\Delta\delta_N/5)^2]^{1/2}$ assuming a one-site binding model, a two-site binding model, or a competitive binding model. The one-site binding model assumes

$$\Delta\delta(N,H)_{av} = \frac{\Delta\delta_{FB}}{2P_0}\left\{(P_0 + L_0 + K_d) - \sqrt{(P_0 + L_0 + K_d)^2 - 4P_0L_0}\right\} \quad (1)$$

where $\Delta\delta_{FB}$ is the chemical shift difference between the free and bound forms and P_0 and L_0 are the total concentrations of KIX and p53, respectively. The two-site binding model was used to analyze the HSQC titrations of AD1 and AD2 into ^{15}N-labeled KIX:

$$\Delta\delta(N) \text{ or } \Delta\delta(H) = \frac{L}{K_{d1} + L}\Delta\delta_1 + \frac{L}{K_{d2} + L}\Delta\delta_2 \quad (2)$$

where K_{d1} and K_{d2} are the dissociation constants for the primary and secondary binding sites, respectively, $\Delta\delta_1$ and $\Delta\delta_2$ are the chemical shift differences between the free form and the bound form with the primary and secondary site occupied, respectively, and L is the concentration of p53 free in solution and is obtained by solving the equation (*44*):

$$L^3 + (2P_0 - L_0 + K_{d1} + K_{d2})L^2 + \{(P_0 - L_0)(K_{d1} + K_{d2}) + K_{d1}K_{d2}\}L - K_{d1}K_{d2}L_0 = 0 \quad (3)$$

A competitive binding model was used for the HSQC titrations of full-length p53 into ^{15}N-labeled KIX:

$$\Delta\delta(N,H)_{av} = \frac{L}{K_{d1}K_{d2} + (K_{d1} + K_{d2})L}(K_{d2}\Delta\delta_1 + K_{d1}\Delta\delta_2) \quad (4)$$

This equation can be transformed into

$$\Delta\delta(N,H)_{av} = \frac{L}{K_d + L}\Delta\delta_m \quad (5)$$

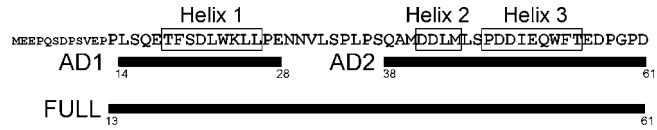

FIGURE 1: Sequence of the N-terminal transactivation domain of p53. The regions that form helical structure in complexes with MDM2 (*52*) and replication protein A (*53*) are boxed. The regions corresponding to the AD1 and AD2 peptides used in this work are indicated by black bars.

Table 1: Dissociation Constants (K_d, μM) Measured by ITC and NMR for the p53 Transactivation Domain with CBP KIX Domain

	ITC[a]	NMR[b]
full p53(1−61)	19 ± 5	
full p53(13−61)	22 ± 5	9.3 ± 0.5
AD1 p53(14−28)	nd[c]	214 ± 5
AD1 p53(14−28) (MLL site)[d]		211 ± 6
AD1 p53(14−28) (pKID/c-Myb site)[e]		242 ± 19
AD2 p53(38−61)	nd[c]	79 ± 4
AD2 p53(38−61) (MLL site)[d]		49 ± 3
AD2 p53(38−61) (pKID/c-Myb site)[e]		94 ± 6
full p53(13−57)pT18		1.8 ± 0.2
full p53(13−57)pS20		1.3 ± 0.2
full p53(13−57)pT18pS20		0.6 ± 0.1
MLL(2840−2858) to KIX[f]	2.8 ± 0.4	
pKID(116−149) to KIX[f]	1.3 ± 0.02	
Myb(291−315) to KIX[f]	10.0 ± 2.0	

[a] ITC measurements were performed at 35 °C, pH 7.0. The K_d for binding of p53(13−61) under NMR conditions (27 °C, pH 6.5) is 8.5 ± 1.0 μM. [b] K_d values from NMR titrations at 27 °C, pH 6.5, were obtained by global analysis. [c] nd, not detectable by ITC. [d] The titration curves of the following residues were used for the semiglobal fitting: 614, 616, 620−626, 631, 666, 669, and 670. [e] The titration curves of the following residues were used for the semiglobal fitting: 595, 596, 600, 608, 609, 650, 652, 654, 655, 657, 661, and 663. [f] K_d values at 27 °C, pH 7.0 (*12*).

$$K_d = \frac{K_{d1}K_{d2}}{K_{d1} + K_{d2}} \quad (6)$$

$$\Delta\delta_m = \frac{(1/K_{d1})\Delta\delta_1 + (1/K_{d2})\Delta\delta_2}{(1/K_{d1}) + (1/K_{d2})} \quad (7)$$

where K_d in eqs 5 and 6 is the harmonic mean of K_{d1} and K_{d2}. Here

$$L = \frac{1}{2}\left\{(L_0 - P_0 - K_d) + \sqrt{(L_0 - P_0 - K_d)^2 + 4K_dL_0}\right\} \quad (8)$$

Equations 5 and 8 hold also in the one-site binding model, except that the K_d for the competitive binding model is the harmonic mean of K_{d1} and K_{d2}.

The titration curves were fitted locally or globally with an in-house fitting program nmrKd using the Levenberg−Marquardt algorithm (*45*).

RESULTS

Interaction between p53 TAD and KIX. In order to dissect the interactions between the p53 TAD and KIX, various p53 TAD constructs, including short peptides representing the subdomains AD1 (residues 14−28) and AD2 (residues 38−61) (Figure 1), were prepared. Unlabeled and ^{15}N- or ^{15}N,^{13}C-labeled p53 TAD (residues 13−61) and KIX domain were expressed in *E. coli* for ITC and NMR experiments. Since the affinities of p53(1−61) and p53(13−61) for KIX are the same within experimental error (Table 1), the shorter construct p53(13−61) was used for the NMR titrations. The

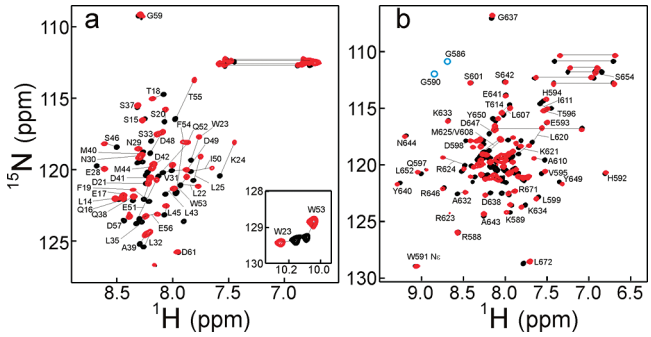

FIGURE 2: ^{1}H−^{15}N HSQC spectra of p53(13−61) and KIX. (a) ^{1}H−^{15}N HSQC spectra of [^{15}N]p53(13−61) free (black) and in the presence of a 2-fold excess of unlabeled KIX (red). (b) ^{1}H−^{15}N HSQC spectra of [^{15}N]KIX free (black) and in the presence of a 2-fold excess of unlabeled p53(13−61) (red). All residues are labeled on the bound (1:2 mol ratio) peaks. Cross-peaks from the two tryptophan side chains of p53 are shown in the inset.

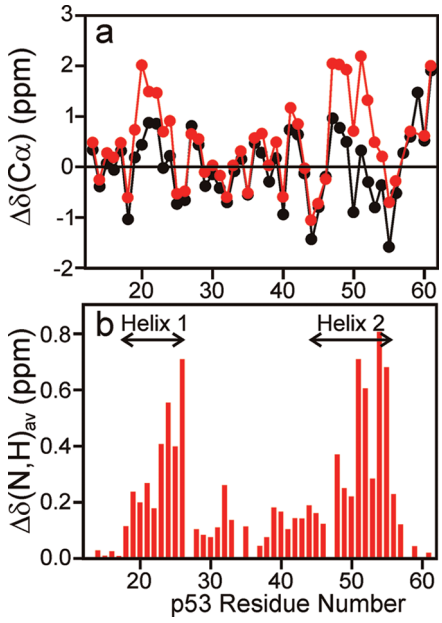

FIGURE 3: Secondary ^{13}Cα chemical shifts and weighted average chemical shift changes of p53(13−61). (a) ^{13}Cα shifts calculated by subtraction of published random coil values from the experimental ^{13}Cα chemical shifts for free p53(13−61) (black dots) and KIX-bound p53(13−61) (red dots). (b) Histogram showing weighted average chemical shift changes $\Delta\delta(N,H)_{av}$ $(=[(\Delta\delta_{HN})^2 + (\Delta\delta_N/5)^2]^{1/2}$, where $\Delta\delta_{HN}$ and $\Delta\delta_N$ correspond to the differences in amide ^{1}H and ^{15}N chemical shifts between the free and bound states) for p53 amide resonances caused by binding to KIX.

^{1}H−^{15}N HSQC titrations of ^{15}N-labeled p53(13−61) with unlabeled KIX and of ^{15}N-labeled KIX with unlabeled p53(13−61) showed that exchange between free and bound forms is fast on the NMR time scale (Supporting Information Figure S4). Although the affinity is modest (22 ± 5 μM) (Table 1), many HSQC cross-peaks of both p53 and KIX are shifted in the titrations, and a subset of resonances undergoes significant changes, suggesting site-specific binding between p53 TAD and KIX.

Folding of p53 TAD upon Interaction with KIX. As reported in previous studies (*21, 46*), the ^{1}H−^{15}N HSQC spectrum of the free p53 TAD shows poorly dispersed ^{1}H resonances (Figure 2a, black), and the ^{13}Cα chemical shifts are close to random coil values (Figure 3a, black points), indicating that the p53 TAD is largely unstructured in the absence of a binding partner. Addition of KIX results in large

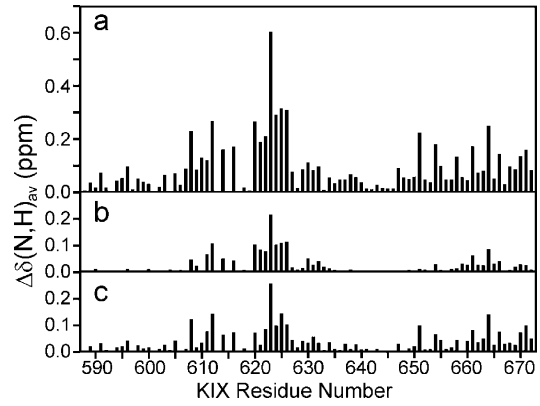

FIGURE 4: Histogram showing weighted average chemical shift changes for KIX amide resonances between free KIX and in the 1:1 complexes with (a) p53(13−61), (b) p53(14−28), and (c) p53(38−61).

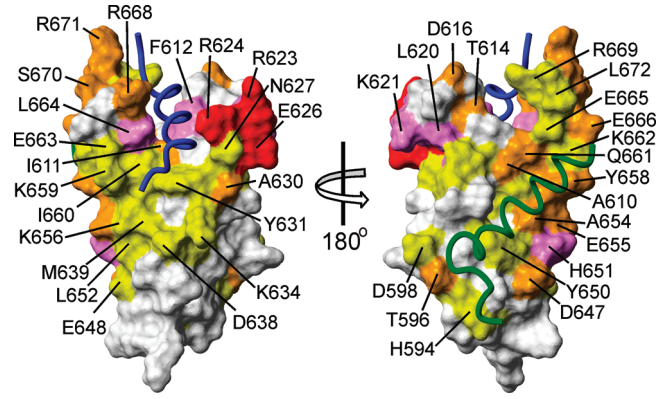

FIGURE 5: Binding sites of p53 TAD on KIX. Weighted average chemical shift differences $\Delta\delta(N,H)_{av}$ of KIX amide resonances (Figure 4a) between free KIX and in complex with p53(13−61) are mapped onto the surface of KIX in the ternary KIX·MLL·c-myb complex (*64*) (PDB 2AGH) using colors to indicate changes in chemical shift greater than 2 × standard deviation from the mean (SD) (red), between 1 and 2 × SD (magenta), between mean and 1 × SD (orange), and between half of the average chemical shift difference ($\Delta\delta_{av}/2$) and the average chemical shift difference ($\Delta\delta_{av}$) (yellow). The polypeptide backbones of the bound MLL and c-Myb are shown in blue and green, respectively. The figure was prepared using MOLMOL (*65*).

shifts of the ^{1}H and ^{15}N resonances (Figure 2a, red) of residues in both the AD1 and AD2 regions (Figure 3b), indicating that both motifs contact KIX in the complex. The Cα secondary chemical shifts of residues 19−24 and 47−53 increase significantly upon KIX binding (Figure 3a, red points), consistent with formation of local helical structure. Similar coupled folding and binding events occur upon binding of the activation domains of pKID or c-Myb to KIX (*47*).

Localization of the p53 TAD Binding Site on KIX. To identify the p53 TAD binding site on KIX, we performed ^{1}H−^{15}N HSQC titrations of unlabeled p53(13−61) into ^{15}N-labeled KIX (Figure 2b). The amide chemical shift changes are plotted in Figure 4a, and residues with amide resonances that are highly perturbed by TAD binding are mapped onto the KIX structure in Figure 5. The chemical shift changes show that the p53(13−61) TAD contacts two regions of the KIX surface. One binding site is in the vicinity of residues F612, R623, R624, E626, L664, and R668, located in the loop between the first and second helix and at the end of the third helix of KIX; this site overlaps the MLL binding site.

The other site is formed by D647, H651, A654, E655, and Y658, which are located on a different face of KIX and constitute part of the pKID/c-Myb binding site. These results suggest that the full-length p53 TAD interacts with the MLL and pKID/c-Myb sites simultaneously.

In order to better define the binding sites of the AD1 and AD2 subdomains of the p53 TAD on KIX, we separately titrated peptides representing the AD1 and AD2 subdomains (p53(14−28) and p53(38−61)) into ^{15}N-labeled KIX. Although AD1 and AD2 binding caused smaller perturbations of the KIX NMR spectrum compared to the full-length TAD, it is clear from the pattern of chemical shift changes that both of the component peptides contact both the MLL and pKID/c-Myb binding sites (Figure 4b,c).

To determine which of the two binding sites was preferred by each subdomain, K_d values were calculated from global fitting of the HSQC titration data, assuming a one-site or two-site binding model. Global fitting of the AD1 and AD2 titrations assuming a one-site binding model converged and gave K_d values of 214 ± 5 and 79 ± 4 μM, respectively (Table 1); the fitting assuming the two-site binding model failed to converge. This could happen if the K_d values for the primary and secondary binding are close. Therefore, the titration curves of residues in the MLL site and those in the pKID/c-Myb site were fitted separately to obtain estimates of the relative binding affinities in each site. It should be noted that the K_d values thus obtained are not true dissociation constants for two-site binding, because the free p53 concentration (L) is different for the one-site and two-site binding models (see eqs 2 and 5). The K_d values for the MLL and the pKID/c-Myb sites are 211 ± 6 and 242 ± 19 μM, respectively, for binding of the AD1 peptide and 49 ± 3 and 94 ± 6 μM for AD2 (Table 1 and Figure 6a,b) These values differ by less than a factor of 2, consistent with the global fitting results. However, it is also important to note that the difference in the two K_d values is larger than the experimental error. Thus, AD1 and AD2 can bind to KIX at two different binding sites with similar K_d values, with binding to the MLL site occurring with slightly higher affinity for each of the subdomains and with AD2 having a greater affinity for both sites than AD1.

The existence of alternate binding modes for the p53 TAD was confirmed by competition experiments (Supporting Information Figure S5) in which unlabeled MLL, pKID, or c-Myb was titrated into the 1:1 ^{15}N-p53(13−61) TAD:^{14}N-KIX binary complex and changes in amide chemical shifts in HSQC spectra were monitored. Resonances associated with both the AD1 and AD2 motifs are shifted back toward their chemical shifts in free p53 TAD spectra, showing that binding of a competitive ligand in either the MLL or c-Myb/pKID binding site inhibits interactions with both p53 binding motifs.

Spin Labels Reveal Nonspecific Interactions between p53 and KIX. Since the AD1 and AD2 motifs can potentially bind to both the MLL and pKID/c-Myb sites of KIX, we next investigated the preferred mode of interaction of the full-length p53 TAD with KIX using site-directed paramagnetic nitroxide spin labeling. ^{1}H−^{15}N HSQC spectra of KIX with N-terminal or C-terminal spin-labeled p53 TAD were collected in both their paramagnetic and diamagnetic forms. Because the spin labels are attached at the flexible N- and C-terminal ends of the p53 TAD, we have not attempted to extract quantitative distances from the data. Rather, we looked for trends in paramagnetic enhancement of nuclear spin relaxation of KIX. Paramagnetic broadening ratios for N-terminal and C-terminal spin labeling of p53 TAD are shown in Figure 7a. Many of the cross-peaks in the HSQC spectra of KIX are significantly broadened by the paramagnetic spin labels on the p53 TAD. The broadening effects are mapped onto the KIX structure in Figure 8. The paramagnetic spin labels attached at the C-terminus of p53(13−61) strongly broaden the amide cross-peaks of residues in both the pKID/c-Myb and MLL binding sites (Figure 8b), showing that the AD2 motif interacts with approximately the same affinity at both binding surfaces of KIX. In addition, the broadening patterns suggest that the AD2 helix binds in two opposing orientations at each binding site. At the pKID/c-Myb site, for example, the spin label causes extensive broadening for residues on both the α_1 helix and α_3 helix, consistent with binding in alternate conformations that differ by an approximately 180° rotation in the orientation of the helix axis. The N-terminal spin label (Figure 8a) broadens the resonances of residues in the MLL site somewhat more strongly than those from the pKID/c-Myb binding surface, indicating that the AD1 motif binds preferentially to the MLL site and only weakly to the other binding surface. Again, the broadening patterns suggest that the AD1 helix is disordered in its interactions with KIX, binding in a minimum of two conformations with approximately antiparallel helix orientations.

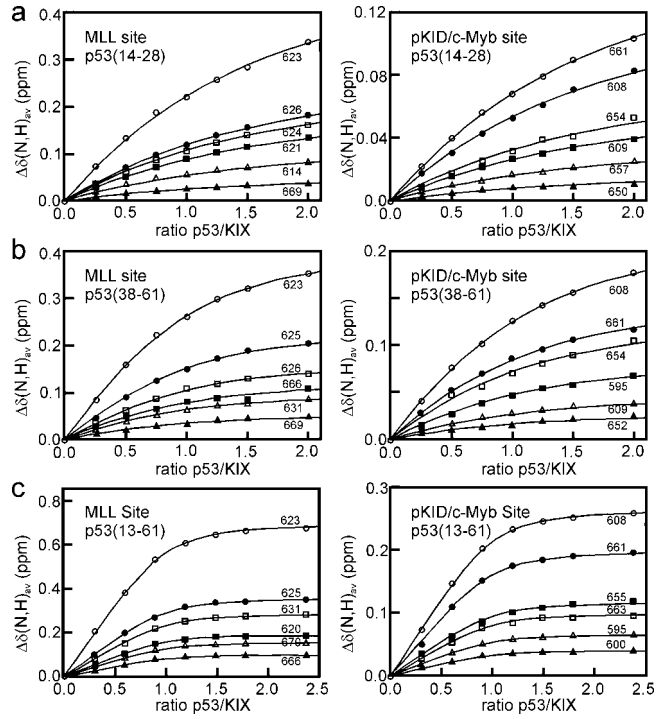

FIGURE 6: Selected HSQC titration curves showing the average of the ^{15}N and ^{1}H chemical shift changes $\Delta\delta(N,H)_{av}$ (=$[(\Delta\delta_{HN})^2 + (\Delta\delta_N/5)^2]^{1/2}$) as a function of concentration ratio for the titration of ^{15}N-labeled KIX with (a) the AD1 peptide p53(14−28), (b) the AD2 peptide p53(38−61), and (c) p53(13−61). The left three plots show the curves corresponding to the MLL binding site (residues 614, 616, 620−626, 631, 666, 669, and 670), while the right three plots show the curves corresponding to the pKID/c-Myb binding site (residues 595, 596, 600, 608, 609, 650, 652, 654, 655, 657, 661, and 663). Values of $\Delta\delta(N,H)_{av}$ are plotted as symbols, and the continuous lines show the curves fitted semiglobally (a, b) or globally (c) to a one-site binding model. The complete set of curves that were used to obtain the global and semiglobal fits is shown in Supporting Information Figure S8.

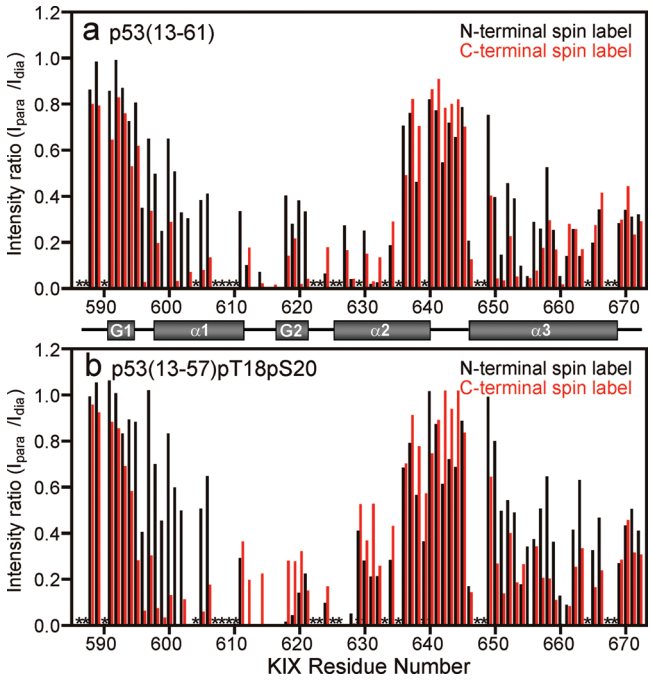

FIGURE 7: Broadening of KIX resonances by spin-labeled p53 peptides. The histograms show the experimental intensity ratios ($I = I_{para}/I_{dia}$) for each residue with an adequately resolved cross-peak in the $^{1}H-^{15}N$ HSQC spectrum of ^{15}N KIX in complex with (a) N-terminal spin-labeled p53(13−61) (black bars) and C-terminal spin-labeled p53(13−61) (red bars) and (b) N-terminal spin-labeled phosphorylated p53(13−57)pT18pS20 (black bars) and C-terminal spin-labeled phosphorylated p53(13−57)pT18pS20 (red bars). An intensity ratio of 1 indicates no effect of the spin label on an amide proton. Residues for which quantitation was not possible due to HSQC cross-peak overlap are indicated with stars (*). The location of the helices (3_{10} helix, G1 and G2; α-helix, α1, α2, and α3) in the structure of KIX is shown schematically between the plots.

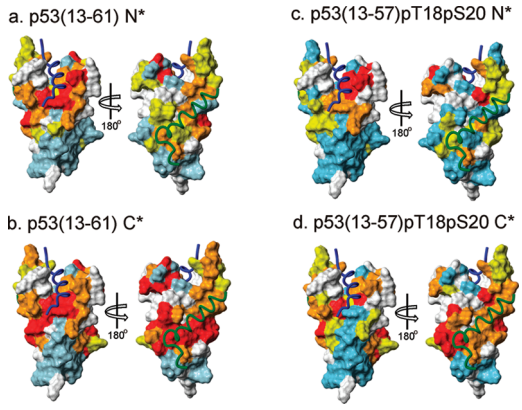

FIGURE 8: Mapping of broadening effects of spin-labeled p53(13−61) and spin-labeled phosphorylated p53(13−57)pT18pS20 on the surface of the KIX domain. The location of residues whose amides show broadening upon binding are indicated by color coding based upon the ratio of amide signal in the paramagnetic sample versus diamagnetic sample (I_{para}/I_{dia}): red = <0.1, orange = 0.1−0.3, yellow = 0.3−0.5, blue = >0.5, and white = residues with overlapped HSQC cross-peaks. The polypeptide backbones of the bound MLL and c-Myb are shown in blue and green, respectively. Panels: (a) N-terminal spin-labeled p53(13−61), (b) C-terminal spin-labeled p53(13−61), (c) N-terminal spin-labeled p53(13−57)pT18pS20, and (d) C-terminal spin-labeled p53(13−57)pT18pS20. The figure was prepared using MOLMOL (*65*).

Thus, the AD1 and AD2 motifs effectively compete for binding to the MLL site of KIX.

Competitive Binding Model for AD1 and AD2 Interactions. An apparent dissociation constant for the binding of the full-length p53 TAD to KIX was estimated to be 9.3 ± 0.5 μM by assuming a one-site binding model and fitting all the HSQC titration curves globally (Table 1, Figure 6c). The K_d value is in excellent agreement with that obtained by ITC (8.5 ± 1 μM) under the same conditions as the NMR titration (27 °C, pH 6.5).

Since the spin-labeling and competition experiments showed the presence of two binding modes at the same binding sites for the interaction of KIX with p53(13−61), fitting to a single site binding model will overestimate the binding affinity. We therefore fit the chemical shift titration data to a competitive two-state binding model (Scheme 1):

Scheme 1

$$[\mathrm{KIX}\cdot\mathrm{p53}]_1 \xleftrightarrow{K_{d1}} \mathrm{KIX} + \mathrm{p53} \xleftrightarrow{K_{d2}} [\mathrm{KIX}\cdot\mathrm{p53}]_2$$

In this model, states 1 and 2 differ in the occupancy of the MLL and pKID/c-Myb binding sites; in one state, AD1 occupies the MLL site and AD2 the pKID/c-Myb site, with the reverse occupancies in the other state. To a first approximation, we assume that the helix orientational disorder revealed by the spin-labeling experiments does not significantly affect the K_d for binding of AD1 or AD2 in each of the sites on KIX. Because the fitting function for competitive binding (eq 4) has the same form as that for the one-site binding model (eqs 5−7), accurate values of K_{d1}, K_{d2}, $\Delta\delta_1$, and $\Delta\delta_2$ cannot be obtained from the fitting. However, values of $\Delta\delta_m$ and K_d (the harmonic mean of K_{d1} and K_{d2}) can be obtained by fitting the data with the one-site binding model. Thus, the apparent K_d obtained by fitting to a one-site binding model (9.3 ± 0.5 μM, Table 1) is the harmonic mean of K_{d1} and K_{d2}. Using this result, we can estimate limits on K_{d1} and K_{d2}. The spin-label experiment shows that cross-peak intensities in both the MLL and pKID/c-Myb sites are decreased to a similar extent, indicating that the populations of the two binding modes are similar. This, in turn, suggests that the K_d values for the two binding modes are similar. Indeed, if $K_{d1} \ll K_{d2}$ (or *vice versa*), then a single binding mode is dominant and the secondary binding mode would not be observed. In the simplest case, if both K_{d1} and K_{d2} are the same, then we get $K_{d1} = K_{d2} = 2K_d = 18.6$ μM from eq 6.

In order to estimate limits on K_{d1} and K_{d2}, we calculated the population of the two binding modes by varying the K_{d1} and K_{d2} values while restraining $K_d = K_{d1}K_{d2}/(K_{d1} + K_{d2}) = 9.3$ μM. With this restraint, K_{d1} and K_{d2} are related (Supporting Information Figure S6a). When the concentrations of both KIX and full-length p53 TAD are fixed at 200 μM (1:1 molar ratio), ~20% of KIX exists as the free (unbound) form, with the remainder in either of the two bound states (Supporting Information Figure S6b). Because the spin-label experiment indicates that the populations of the two binding modes are comparable, we can safely assume that the ratio of the populations of the two binding modes should be between 0.5 and 2.0. Accordingly, K_{d1} and K_{d2} are estimated to be 14−27 μM and 27−14 μM, respectively (Supporting Information Figure S6c).

Enhancement of Binding Affinity and Specificity by Phosphorylation. Phosphorylation of the p53 TAD at Thr18 results in a 5-fold increase in the binding affinity for the KIX domain

relative to unphosphorylated p53(13−61) (Table 1). A comparable increase in binding affinity is observed upon phosphorylation at Ser20. Since simultaneous phosphorylation of Ser15 and Ser20, or Thr18 and Ser20, appears to have a synergistic role in activating p53-mediated apoptosis (*48*−*50*), we investigated binding of a doubly phosphorylated peptide (p53(13−57)pT18pS20) to the KIX domain; this peptide binds with ∼15-fold higher affinity than the unphosphorylated p53 TAD (Table 1).

To investigate the effect of phosphorylation on the mode of p53 TAD interaction with KIX, we prepared N-terminal and C-terminal spin-labeled samples of doubly phosphorylated p53(13−57)pT18pS20 and measured the broadening of KIX HSQC cross-peaks caused by the paramagnetic spin labels. Paramagnetic broadening ratios for N-terminal and C-terminal spin-labeled samples of the phosphorylated p53 TAD are shown in Figure 7b, and the results are mapped onto the KIX structure in Figure 8c,d. The spin-label experiments with the unphosphorylated p53 TAD showed that AD1 and AD2 motifs bind with comparable affinity in both the MLL and pKID/c-Myb sites of KIX, with just a slight preference of the AD1 subdomain for the MLL site. In addition, the broadening induced by N- and C-terminal spin label is similar (Figure 7a). The broadening induced by spin labels on the doubly phosphorylated p53 peptide is much more specific. Cross-peaks of residues in the G1, α1, and α3 helices located in the pKID/c-Myb site of KIX are much more extensively broadened by the C-terminal spin label than by the N-terminal spin label (Figure 7b). Conversely, the N-terminal spin label causes extensive broadening of resonances corresponding to the MLL site (especially in the G2 helix), and much less broadening of cross-peaks from the pKID/c-Myb site than does the N-terminal spin-labeled unphosphorylated p53 TAD (compare panels a and b of Figure 7 in the region of the G2 and α3 helices and panels a and c of Figure 8).

The C-terminal spin label on the phosphorylated p53 TAD causes more broadening in the pKID/c-Myb site and less in the MLL site than its unphosphorylated counterpart (Figures 7 and 8b,d). Based on the observed changes in K_d and the increased specificity of the broadening effects of the spin labels, it is evident that phosphorylation of the p53 TAD in the AD1 region enhances the specificity of binding to the KIX domain as well as enhancing the affinity (Table 1).

DISCUSSION

KIX provides two distinct binding surfaces for interactions with transcriptional activation domains. MLL, Tax, Tat, and c-Jun bind primarily to a groove formed at the interface between helices G2, α_2, and α_3 (at the top of the KIX domain in the view shown in Figures 5 and 8), while pKID and c-Myb bind preferentially to a hydrophobic groove across the surfaces of helices α_1 and α_3, on the opposite face of KIX from the MLL site (Figures 5 and 8). Activation domains from the two groups bind simultaneously and cooperatively to KIX with a 2-fold enhanced affinity (*12*). Unlike other transcription factors, the p53 TAD interacts with both of the KIX binding sites with similar affinity, employing both the AD1 and AD2 subdomains. The affinity is estimated to be ∼14−27 μM based on fitting the chemical shift titrations to a competitive model for binding of the full-length p53 TAD. The full-length p53 TAD is intrinsically disordered (*20*, *21*). The AD1 and AD2 subdomains each contain an amphipathic *ϕ*-x-x-*ϕ*-*ϕ* motif (*ϕ* = bulky hydrophobic residue and x = any residue), which mediates interactions with target proteins, and several acidic residues. These sequence characteristics are common in transactivation domains and are conserved in many KIX binding proteins (Figure 9). The primary sequence similarity indicates that KIX binding proteins have the potential to bind both the MLL and pKID/c-Myb sites through their amphipathic motifs. Indeed, both pKID (*51*) and c-Myb (unpublished data) can bind to the MLL binding site with low affinity in addition to binding in their cognate, high-affinity site.

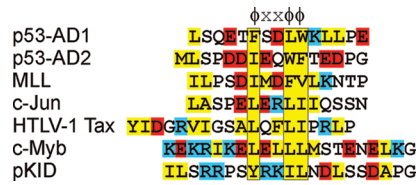

FIGURE 9: Alignment of the amino acid sequences of KIX binding proteins. Conserved amino acids are colored according to type: hydrophobic residues (A, V, I, L, M) are shown in yellow, positively charged residues (R, K) in blue, and negatively charged residues (D, E) in red.

The amphipathic motifs within the AD1 and AD2 regions of the p53 TAD fold into local helical structure upon binding to KIX (Figure 3a). The intervening ∼20-residue loop does not appear to interact significantly with KIX since resonances from this region experience only very small chemical shift perturbations upon binding (Figure 3). This loop functions as a flexible linker that is critical for increasing the binding affinity of the full-length p53 TAD by increasing the effective local concentration of AD1 and AD2. In agreement with this notion, HSQC titrations showed that the chemical shift perturbations induced in the KIX spectrum by the addition of a mixture of the isolated AD1 and AD2 peptides are smaller than those caused by binding of the full-length TAD (Supporting Information Figure S7). The AD1 and AD2 motifs have also been observed to fold into helical structure upon binding to MDM2, replication protein A, and the p62/Tfb1 subunit of TFIIH (*52*−*54*).

The full-length p53 TAD binds KIX with significantly enhanced affinity relative to the isolated AD1 and AD2 domains, despite the lack of specificity and accompanying disorder in the local interactions. The overall affinity for p53(13−61) is significantly higher (K_d = 14−27 μM from the competitive binding model) than for binding of either of the isolated AD1 or AD2 motifs (Table 1), suggesting that the two motifs bind cooperatively and synergistically to KIX. Nevertheless, AD2 appears to dominate the interaction since it binds with 50 and 100 μM K_d to the MLL and pKID/c-Myb sites, respectively, even as an isolated peptide.

Single site phosphorylation at Thr18 or Ser20 of the p53 TAD significantly enhances the affinity for binding to KIX (Table 1). The p53 TAD becomes phosphorylated at these and other sites in the AD1 region in response to DNA damage and other forms of genotoxic stress (*15*, *55*, *56*). Phosphorylation of the TAD stabilizes p53 by inhibiting MDM2-mediated degradation and enhances its transcriptional activity and ability to recruit CBP/p300 (*57*−*61*). Consistent with growing evidence that two-site phosphorylation at Thr18 and Ser20 plays a synergistic role in p53 activation

(*48, 50*), binding of a doubly phosphorylated peptide p53(13−57)pT18pS20 to the KIX domain is enhanced 15-fold relative to the unphosphorylated TAD, and the spin-label data illustrated in Figure 8 show that the interactions with KIX become significantly more specific. It thus appears that the KIX domain could play an important role in the regulation of the p53-CBP/p300 interaction by acting as a sensor of phosphorylation state of the p53 TAD.

Specific recognition of phosphorylated peptides by KIX is not without precedent. The KIX domain binds the kinase-inducible activation domain (KID) of the transcription factor CREB in a phosphorylation-dependent manner (*2, 62*). Phosphorylation of KID results in a 40−100-fold increase in binding affinity for KIX (*47*). The enhancement of binding affinity upon phosphorylation of the p53 TAD is more modest (5 −15-fold, Table 1), depending on whether the TAD is phosphorylated at one or two sites. Nevertheless, the binding affinity of all of the phospho-p53 peptides assayed in this work (0.6−2 μM) is comparable to the affinity for binding of pKID to KIX (*47*), i.e., in a range that is biologically relevant. It is important to note that the KIX binding surface utilized by the phosphorylated activation domains differs for p53 and pKID. The pKID binds to the hydrophobic groove across the face of helices α_1 and α_3 of KIX, and the phosphoryl group on Ser133 forms stabilizing hydrogen-bonding interactions with the side chain of Tyr658 of KIX (*9*). In contrast, the phosphorylated AD1 motif of p53 appears to interact preferentially in the MLL binding site on the opposite face of KIX.

The present studies provide new insights into the interplay between CBP/p300 and other regulatory proteins in mediating the p53 response. Control of transcriptional activation appears to reside at least in part on competition between the activation domains of different regulatory proteins for binding to the CBP KIX domain. Our studies show that the KIX domain may act as a phosphorylation sensor, binding p53 phosphorylated at Thr18 and/or Ser20 with enhanced affinity and competing effectively with MDM2 for binding the p53 TAD; phosphorylation at Thr18 or at both Thr18 and Ser20 significantly weakens the binding between the AD1 subdomain and MDM2 (K_d ~3 μM) (*58*) such that KIX can now compete for the p53 TAD (K_d 0.6−2 μM). Other examples include the oncoprotein Tax, which binds to the MLL site of KIX and competes with MLL (*14*). In cancer development, Tax inhibits p53 function by directly competing with it for binding to KIX (*31*). The c-*myb* proto-oncogene product (c-Myb) is essential for cellular proliferation of immature hematopoietic cells, whereas p53 inhibits cell cycle progression. p53 is known to suppress c-Myb-induced transcription and transformation by recruiting mSin3A to downregulate specific Myb target genes (*63*), but since our studies show that c-Myb competes directly with the p53 TAD for KIX binding, it is interesting to speculate that c-Myb suppression may also occur via direct competition for recruitment of CBP/p300.

ACKNOWLEDGMENT

We thank Mindy Landes and Euvel Manlapaz for help with sample preparation and Drs. John Chung and Gerard Kroon for expert assistance with NMR data collection.

SUPPORTING INFORMATION AVAILABLE

HPLC traces and mass spectrometry data establishing the integrity of the spin-labeled peptides (Figures S1 and S2), control experiments showing that free MTSL spin label does not broaden KIX resonances (Figure S3), NMR titrations of KIX and p53 (Figure S4), NMR competition experiments between p53(13−61), MLL, and c-Myb or pKID (Figure S5), relationship between K_{d1} and K_{d2} (Figure S6), chemical shift changes of KIX upon addition of p53(13−61) (Figure S7), and HSQC titration curves (Figure S8). This material is available free of charge via the Internet at http://pubs.acs.org.

REFERENCES

1. Goodman, R. H., and Smolik, S. (2000) CBP/p300 in cell growth, transformation, and development. *Genes Dev. 14*, 1553–1577.
2. Chrivia, J. C., Kwok, R. P., Lamb, N., Hagiwara, M., Montminy, M., and Goodman, R. H. (1993) Phosphorylated CREB binds specifically to nuclear protein CBP. *Nature 365*, 855–859.
3. Giordano, A., and Avantaggiati, M. L. (1999) p300 and CBP: Partners for life and death. *J. Cell. Phys. 181*, 218–230.
4. Ernst, P., Wang, J., Huang, M., Goodman, R. H., and Korsmeyer, S. J. (2001) MLL and CREB bind cooperatively to the nuclear coactivator CREB-binding protein. *Mol. Cell. Biol. 21*, 2249–2258.
5. Bannister, A. J., Oehler, T., Wilhelm, D., Angel, P., and Kouzarides, T. (1995) Stimulation of c-Jun activity by CBP: c-Jun residues Ser63/73 are required for CBP induced stimulation *in vivo* and CBP binding *in vitro*. *Oncogene 11*, 2509–2514.
6. Dai, P., Akimaru, H., Tanaka, Y., Hou, D. X., Yasukawa, T., Kanei-Ishii, C., Takahashi, T., and Ishii, S. (1996) CBP as a transcriptional coactivator of c-Myb. *Genes Dev. 10*, 528–540.
7. Kwok, R. P. S., Laurance, M. E., Lundblad, J. R., Goldman, P. S., Shih, H., Connor, L. M., Marriott, S. J., and Goodman, R. H. (1996) Control of cAMP-regulated enhancers by the viral transactivator Tax through CREB and the co-activator CBP. *Nature 380*, 642–646.
8. Vendel, A. C., and Lumb, K. J. (2003) Molecular recognition of the human coactivator CBP by the HIV-1 transcriptional activator Tat. *Biochemistry 42*, 910–916.
9. Radhakrishnan, I., Pérez-Alvarado, G. C., Parker, D., Dyson, H. J., Montminy, M. R., and Wright, P. E. (1997) Solution structure of the KIX domain of CBP bound to the transactivation domain of CREB: A model for activator:coactivator interactions. *Cell 91*, 741–752.
10. Zor, T., De Guzman, R. N., Dyson, H. J., and Wright, P. E. (2004) Solution structure of the KIX domain of CBP bound to the transactivation domain of c-Myb. *J. Mol. Biol. 337*, 521–534.
11. Campbell, K. M., and Lumb, K. J. (2002) Structurally distinct modes of recognition of the KIX domain of CBP by Jun and CREB. *Biochemistry 41*, 13956–13964.
12. Goto, N. K., Zor, T., Martinez-Yamout, M., Dyson, H. J., and Wright, P. E. (2002) Cooperativity in transcription factor binding to the coactivator CREB-binding protein (CBP). The mixed lineage leukemia protein (MLL) activation domain binds to an allosteric site on the Kix domain. *J. Biol. Chem. 277*, 43168–43174.
13. Vendel, A. C., McBryant, S. J., and Lumb, K. J. (2003) KIX-mediated assembly of the CBP-CREB-HTLV-1 tax coactivator-activator complex. *Biochemistry 42*, 12481–12487.
14. Ramirez, J. A., and Nyborg, J. K. (2007) Molecular characterization of HTLV-1 Tax interaction with the KIX domain of CBP/p300. *J. Mol. Biol. 372*, 958–969.
15. Bode, A. M., and Dong, Z. (2004) Post-translational modification of p53 in tumorigenesis. *Nat. Rev. Cancer 4*, 793–805.
16. Vousden, K. H., and Lane, D. P. (2007) p53 in health and disease. *Nat. Rev. Mol. Cell. Biol. 8*, 275–283.
17. Grossman, S. R. (2001) p300/CBP/p53 interaction and regulation of the p53 response. *Eur. J. Biochem. 268*, 2773–2778.
18. Moll, U. M., and Petrenko, O. (2003) The MDM2-p53 interaction. *Mol. Cancer Res. 1*, 1001–1008.
19. Chang, J., Kim, D. H., Lee, S. W., Choi, K. Y., and Sung, Y. C. (1995) Transactivation ability of p53 transcriptional activation domain is directly related to the binding affinity to TATA-binding protein. *J. Biol. Chem. 270*, 25014–25019.

20. Ayed, A., Mulder, F. A., Yi, G. S., Lu, Y., Kay, L. E., and Arrowsmith, C. H. (2001) Latent and active p53 are identical in conformation. *Nat. Struct. Biol. 8*, 756–760.
21. Dawson, R., Muller, L., Dehner, A., Klein, C., Kessler, H., and Buchner, J. (2003) The N-terminal domain of p53 is natively unfolded. *J. Mol. Biol. 332*, 1131–1141.
22. Unger, T., Mietz, J. A., Scheffner, M., Yee, C. L., and Howley, P. M. (1993) Functional domains of wild-type and mutant p53 proteins involved in transcriptional regulation, transdominant inhibition, and transformation suppression. *Mol. Cell. Biol. 13*, 5186–5194.
23. Candau, R., Scolnick, D. M., Darpino, P., Ying, C. Y., Halazonetis, T. D., and Berger, S. L. (1997) Two tandem and independent sub-activation domains in the amino terminus of p53 require the adaptor complex for activity. *Oncogene 15*, 807–816.
24. Venot, C., Maratrat, M., Sierra, V., Conseiller, E., and Debussche, L. (1999) Definition of a p53 transactivation function-deficient mutant and characterization of two independent p53 transactivation subdomains. *Oncogene 18*, 2405–2410.
25. Zhu, J., Zhang, S., Jiang, J., and Chen, X. (2000) Definition of the p53 functional domains necessary for inducing apoptosis. *J. Biol. Chem. 275*, 39927–39934.
26. Avantaggiati, M. L., Ogryzko, V., Gardner, K., Giordano, A., Levine, A., and Kelly, K. (1997) Recruitment of p300/CBP in p53-dependent signal pathways. *Cell 89*, 1175–1184.
27. Lill, N. L., Grossman, S. R., Ginsberg, D., DeCaprio, J., and Livingston, D. M. (1997) Binding and modulation of p53 by p300/CBP coactivators. *Nature 387*, 823–827.
28. Gu, W., Shi, X. L., and Roeder, R. G. (1997) Synergistic activation of transcription by CBP and p53. *Nature 387*, 819–823.
29. Scolnick, D. M., Chehab, N. H., Stavridi, E. S., Lien, M. C., Caruso, L., Moran, E., Berger, S. L., and Halazonetis, T. D. (1997) CREB-binding protein and p300/CBP-associated factor are transcriptional coactivators of the p53 tumor suppressor protein. *Cancer Res. 57*, 3693–3696.
30. Livengood, J. A., Scoggin, K. E. S., van Orden, K., McBryant, S. J., Edayathumangalam, R. S., Laybourn, P. J., and Nyborg, J. K. (2002) p53 transcriptional activity Is mediated through the SRC1-interacting domain of CBP/p300. *J. Biol. Chem. 277*, 9054–9061.
31. van Orden, K., Giebler, H. A., Lemasson, I., Gonzales, M., and Nyborg, J. K. (1999) Binding of p53 to the KIX domain of CREB binding protein—A potential link to human T-cell leukemia virus, type I-associated leukemogenesis. *J. Biol. Chem. 274*, 26321–26328.
32. Grossman, S. R., Perez, M., Kung, A. L., Joseph, M., Mansur, C., Xiao, Z. X., Kumar, S., Howley, P. M., and Livingston, D. M. (1998) p300/MDM2 complexes participate in MDM2-mediated p53 degradation. *Mol. Cell 2*, 405–415.
33. Wadgaonkar, R., and Collins, T. (1999) Murine double minute (MDM2) blocks p53-coactivator interaction, a new mechanism for inhibition of p53-dependent gene expression. *J. Biol. Chem. 274*, 13760–13767.
34. Teufel, D. P., Freund, S. M., Bycroft, M., and Fersht, A. R. (2007) Four domains of p300 each bind tightly to a sequence spanning both transactivation subdomains of p53. *Proc. Natl. Acad. Sci. U.S.A. 104*, 7009–7014.
35. Giebler, H. A., Loring, J. E., van Orden, K., Colgin, M. A., Garrus, J. E., Escudero, K. W., Brauweiler, A., and Nyborg, J. K. (1997) Anchoring of CREB binding protein to the human T-cell leukemia virus type 1 promoter: a molecular mechanism of Tax transactivation. *Mol. Cell. Biol. 17*, 5156–5164.
36. Harrod, R., Tang, Y., Nicot, C., Lu, H. S., Vassilev, A., Nakatani, Y., and Giam, C. Z. (1998) An exposed KID-like domain in human T-cell lymphotropic virus type 1 Tax is responsible for the recruitment of coactivators CBP/p300. *Mol. Cell. Biol. 18*, 5052–5061.
37. Ariumi, Y., Kaida, A., Lin, J. Y., Hirota, M., Masui, O., Yamaoka, S., Taya, Y., and Shimotohno, K. (2000) HTLV-1 Tax oncoprotein represses the p53-mediated *trans*-activation function through coactivator CBP sequestration. *Oncogene 19*, 1491–1499.
38. Chaudhry, S., Freebern, W. J., Smith, J. L., Butscher, W. G., Haggerty, C. M., and Gardner, K. (2002) Cross-tegulation of T cell growth factor expression by p53 and the Tax oncogene. *J. Immunol. 169*, 6767–6778.
39. Sugase, K., Landes, M. A., Wright, P. E., and Martinez-Yamout, M. (2008) Overexpression of post-translationally modified peptides in *Escherichia coli* by co-expression with modifying enzymes. *Protein Expression Purif. 57*, 108–115.
40. Delaglio, F., Grzesiek, S., Vuister, G. W., Guang, Z., Pfeifer, J., and Bax, A. (1995) NMRPipe: a multidimensional spectral processing system based on UNIX pipes. *J. Biomol. NMR 6*, 277–293.
41. Johnson, B. A., and Blevins, R. A. (1994) NMRView: A computer program for the visualization and analysis of NMR data. *J. Biomol. NMR 4*, 604–613.
42. Grzesiek, S., and Bax, A. (1992) Improved 3D triple-resonance NMR techniques applied to a 31 kDa protein. *J. Magn. Reson. 96*, 432–440.
43. Wittekind, M., and Mueller, L. (1993) HNCACB, a high-sensitivity 3D NMR experiment to correlate amide-proton and nitrogen resonances with the alpha- and beta-carbon resonances in proteins. *J. Magn. Reson. 101*, 201–205.
44. Wang, Z. X., and Jiang, R. F. (1996) A novel two-site binding equation presented in terms of the total ligand concentration. *FEBS Lett. 392*, 245–249.
45. Press,W. H., Teukolsky, S. A., Vetterling, W. T., and Flannery, B. P. (1992) *Numerical Recipes in C*, Cambridge University Press, Cambridge, U.K.
46. Lee, H., Mok, K. H., Muhandiram, R., Park, K. H., Suk, J. E., Kim, D. H., Chang, J., Sung, Y. C., Choi, K. Y., and Han, K. H. (2000) Local structural elements in the mostly unstructured transcriptional activation domain of human p53. *J. Biol. Chem. 275*, 29426–29432.
47. Zor, T., Mayr, B. M., Dyson, H. J., Montminy, M. R., and Wright, P. E. (2002) Roles of phosphorylation and helix propensity in the binding of the KIX domain of CREB-binding protein by constitutive (c-Myb) and inducible (CREB) activators. *J. Biol. Chem. 277*, 42241–42248.
48. Jabbur, J. R., and Zhang, W. (2002) p53 antiproliferative function is enhanced by aspartate substitution at threonine 18 and serine 20. *Cancer Biol. Ther. 1*, 277–283.
49. Chao, C., Herr, D., Chun, J., and Xu, Y. (2006) Ser18 and 23 phosphorylation is required for p53-dependent apoptosis and tumor suppression. *EMBO J. 25*, 2615–2622.
50. Nakamizo, A., Amano, T., Zhang, W., Zhang, X. Q., Ramdas, L., Liu, T. J., Bekele, B. N., Shono, T., Sasaki, T., Benedict, W. F., Sawaya, R., and Lang, F. F. (2008) Phosphorylation of Thr18 and Ser20 of p53 in Ad-p53-induced apoptosis. *Neuro-oncol. 10*, 275–291.
51. Sugase, K., Dyson, H. J., and Wright, P. E. (2007) Mechanism of coupled folding and binding of an intrinsically disordered protein. *Nature 447*, 1021–1025.
52. Kussie, P. H., Gorina, S., Marechal, V., Elenbaas, B., Moreau, J., Levine, A. J., and Pavletich, N. P. (1996) Structure of the MDM2 oncoprotein bound to the p53 tumor suppressor transactivation domain. *Science 274*, 948–953.
53. Bochkareva, E., Kaustov, L., Ayed, A., Yi, G. S., Lu, Y., Pineda-Lucena, A., Liao, J. C. C., Okorokov, A. L., Milner, J., Arrowsmith, C. H., and Bochkarev, A. (2005) Single-stranded DNA mimicry in the p53 transactivation domain interaction with replication protein A. *Proc. Natl. Acad. Sci. U.S.A. 102*, 15412–15417.
54. Di Lello, P., Jenkins, L. M. M., Jones, T. N., Nguyen, B. D., Hara, T., Yamaguchi, H., Dikeakos, J. D., Appella, E., Legault, P., and Omichinski, J. G. (2006) Structure of the Tfb1/p53 complex: insights into the interaction between the p62/Tfb1 subunit of TFIIH and the activation domain of p53. *Mol. Cell 22*, 731–740.
55. Appella, E., and Anderson, C. W. (2001) Post-translational modifications and activation of p53 by genotoxic stresses. *Eur. J. Biochem. 268*, 2764–2772.
56. Xu, Y. (2003) Regulation of p53 responses by post-translational modifications. *Cell Death Differ. 10*, 400–403.
57. Sakaguchi, K., Saito, S., Higashimoto, Y., Roy, S., Anderson, C. W., and Appella, E. (2000) Damage-mediated phosphorylation of human p53 threonine 18 through a cascade mediated by a casein 1-like kinase. Effect on Mdm2 binding. *J. Biol. Chem. 275*, 9278–9283.
58. Schon, O., Friedler, A., Bycroft, M., Freund, S. M., and Fersht, A. R. (2002) Molecular mechanism of the interaction between MDM2 and p53. *J. Mol. Biol. 323*, 491–501.
59. Dumaz, N., and Meek, D. W. (1999) Serine15 phosphorylation stimulates p53 transactivation but does not directly influence interaction with HDM2. *EMBO J. 18*, 7002–7010.
60. Lambert, P. F., Kashanchi, F., Radonovich, M. F., Shiekhattar, R., and Brady, J. N. (1998) Phosphorylation of p53 serine 15 increases interaction with CBP. *J. Biol. Chem. 273*, 33048–33053.

61. Dornan, D., and Hupp, T. R. (2001) Inhibition of p53-dependent transcription by BOX-I phospho-peptide mimetics that bind to p300. *EMBO Rep. 2*, 139–144.
62. Parker, D., Ferreri, K., Nakajima, T., LaMorte, V. J., Evans, R., Koerber, S. C., Hoeger, C., and Montminy, M. (1996) Phosphorylation of CREB at Ser133 induces complex formation with CPB via a direct mechanism. *Mol. Cell. Biol. 16*, 694–703.
63. Tanikawa, J., Nomura, T., Macmillan, E. M., Shinagawa, T., Jin, W., Kokura, K., Baba, D., Shirakawa, M., Gonda, T. J., and Ishii, S. (2004) p53 suppresses c-Myb-induced trans-activation and transformation by recruiting the corepressor mSin3A. *J. Biol. Chem. 279*, 55393–55400.
64. De Guzman, R. N., Goto, N. K., Dyson, H. J., and Wright, P. E. (2006) Structural basis for cooperative transcription factor binding to the CBP coactivator. *J. Mol. Biol. 355*, 1005–1013.
65. Koradi, R., Billeter, M., and Wüthrich, K. (1996) MOLMOL: A program for display and analysis of macromolecular structures. *J. Mol. Graphics 14*, 51–55.

BI802055V